Identifying radiotherapy target volumes in brain cancer by image analysis

Kun Cheng[1], Dean Montgomery[1], Yang Feng[1], Robin Steel[1], Hanqing Liao[2], Duncan B. McLaren[3], Sara C. Erridge[3], Stephen McLaughlin[4], William H. Nailon[1,5] ✉

[1]*Department of Oncology Physics, Edinburgh Cancer Centre, Western General Hospital, Crewe Road South, Edinburgh EH4 2XU, UK*
[2]*Department of Electrical Engineering and Electronics, University of Liverpool, Liverpool L69 3GQ, UK*
[3]*Department of Clinical Oncology, Edinburgh Cancer Centre, Western General Hospital, Crewe Road South, Edinburgh EH4 2XU, UK*
[4]*School of Engineering and Physical Sciences, Heriot Watt University, David Brewster Building, Edinburgh EH14 4AS, UK*
[5]*School of Engineering, University of Edinburgh, King's Buildings, Mayfield Road, Edinburgh EH9 3JL, UK*
✉ *E-mail: W.Nailon@ed.ac.uk*

Published in Healthcare Technology Letters; Received on 26th March 2015; Revised on 4th August 2015; Accepted on 11th August 2015

To establish the optimal radiotherapy fields for treating brain cancer patients, the tumour volume is often outlined on magnetic resonance (MR) images, where the tumour is clearly visible, and mapped onto computerised tomography images used for radiotherapy planning. This process requires considerable clinical experience and is time consuming, which will continue to increase as more complex image sequences are used in this process. Here, the potential of image analysis techniques for automatically identifying the radiation target volume on MR images, and thereby assisting clinicians with this difficult task, was investigated. A gradient-based level set approach was applied on the MR images of five patients with grades II, III and IV malignant cerebral glioma. The relationship between the target volumes produced by image analysis and those produced by a radiation oncologist was also investigated. The contours produced by image analysis were compared with the contours produced by an oncologist and used for treatment. In 93% of cases, the Dice similarity coefficient was found to be between 60 and 80%. This feasibility study demonstrates that image analysis has the potential for automatic outlining in the management of brain cancer patients, however, more testing and validation on a much larger patient cohort is required.

1. Introduction: Radiotherapy is the core treatment modality in the management of high- and low-grade glioma but the radiation doses required to optimise local control have the potential to affect adjacent normal tissues [1–3]. Consequently, accurate delineation of the radiotherapy target is particularly important. A number of studies have been performed that highlight the challenges of delineation of the gross tumour volume (GTV) and clinical target volume (CTV) in patients with brain cancer [4–8]. Not only does the abnormality on the radiotherapy planning computerised tomography (CT) and registered magnetic resonance (MR) images need to be accurately defined, but also the areas of likely anatomic spread need to be appreciated. The level of difficulty faced by clinicians in carrying out this task is evident in Fig. 1. This shows the extent of grade II, (left), grade III (middle) and grade IV (right) gliomas on MR images where disease can be identified and on CT where it is more difficult to identify. At present, clinicians must use their experience to define the GTV or CTV from analysis of both datasets, a process that is complicated by the fact that the size and shape of the GTV may appear different, sometimes quite significantly, depending on the imaging modality used to visualise the tumour [9, 10]. As a result, significant variability has been reported in the manual segmentation of brain tumours: intra-rater, $20 \pm 15\%$; inter-rater, $28 \pm 12\%$ [11].

Image analysis approaches have the potential to assist clinicians with this difficult task by improving the consistency of target delineation and providing solutions for automatic segmentation of intra-cranial structures on MR image volumes. This has received considerable attention over the past two decades with comprehensive coverage of the important contributions in the field prior to 2007 available in [12]. Contributions thereafter until the present day can be found in [13]. One commonly used method for segmenting intra-cranial MR image structures is to register to an anatomical atlas that contains information on the general shape and form of the structures of interest. By projecting the MR image structures available from the atlas onto the MR image volume under investigation, segmentation is performed [14, 15]. Prastawa *et al.* [16] adopted this approach by first registering to an atlas of healthy brains in their framework for automatically segmenting brain tumours on MR image volumes. Cuadra *et al.* [17] used a similar approach by first registering to an atlas and including a model of lesion growth. The method proved useful in the segmentation of grossly deformed cerebral structures. Wang *et al.* also used prior probabilities from the International Consortium for Brain Mapping together with normalised Gaussian mixture models of grey and white matter and cerebrospinal fluid to establish a Gaussian Bayesian classifier (GBC). The GBC was used to initialise a three-dimensional (3D) fluid vector flow algorithm, which was used for brain tumour segmentation [18]. The approach was validated on publicly available datasets and the Tanimoto distance metric used to assess performance. The findings reported closely matched those of Corso *et al.* [19].

When a suitable atlas is not available, as is generally the case with tumour segmentation, pixel- or voxel-based methods such as level sets [20] or active contour-based approaches [21] can be used. However, these methods require careful initialisation to avoid propagation across weak or missing boundaries, as shown in Fig. 2 (left) [22]. Here, we present the preliminary findings of a pilot study investigating a level set-based approach, which uses limited prior information, for the segmentation of the significant tumour volume, or GTV, on the MR images of five brain cancer patients. Using this approach, the GTV could then be mapped to the corresponding CT for radiotherapy planning.

2. Materials and methods

2.1. Case selection, image acquisition and treatment: Five brain cancer patients (glioma grades II, III and IV), previously treated at the Edinburgh Cancer Centre were selected for this study. To

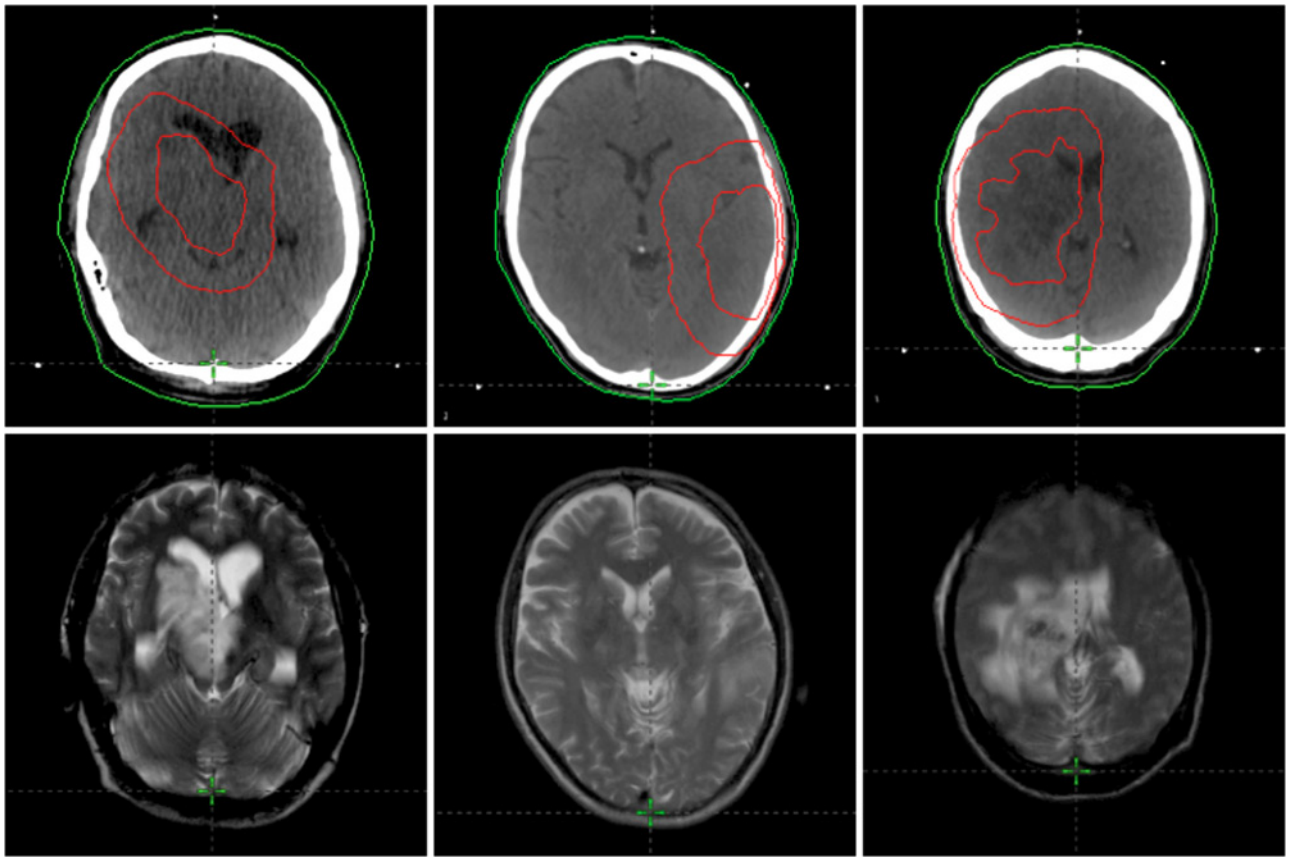

Fig. 1 *Extent of grade II, (left), grade III (middle) and grade IV (right) glioma on registered CT (top) and T2-weighted axial MR (bottom) images. The green contour visible on the CT images is the body contour used for radiotherapy planning. The outer red contour is the PTV, which takes account of variations in size, shape and position, and the inner red contour is the GTV [9, 10]*

ensure geometric reproducibility, patients were immobilised with a thermoplastic mask that was used during CT acquisition and at each fraction during treatment. All CT data was acquired on a single slice General Electric (GE) HiSpeed Fx/i CT scanner (GE Medical Systems, Milwaukee, WI, USA). Pixel resolution in the transaxial plane was 0.977 mm with a 12-bit grey-level range. All MR images were acquired on a Siemens Symphony 1.5 Tesla scanner (Siemens, Munich, Germany) at 5 mm slice thickness and a 12-bit grey-level range. Using an intensity-based method, the CT images were rigidly registered to the MR images with the Mirada Medical Systems registration platform (Mirada Medical Ltd., Oxford, UK) and the registration accuracy independently assessed

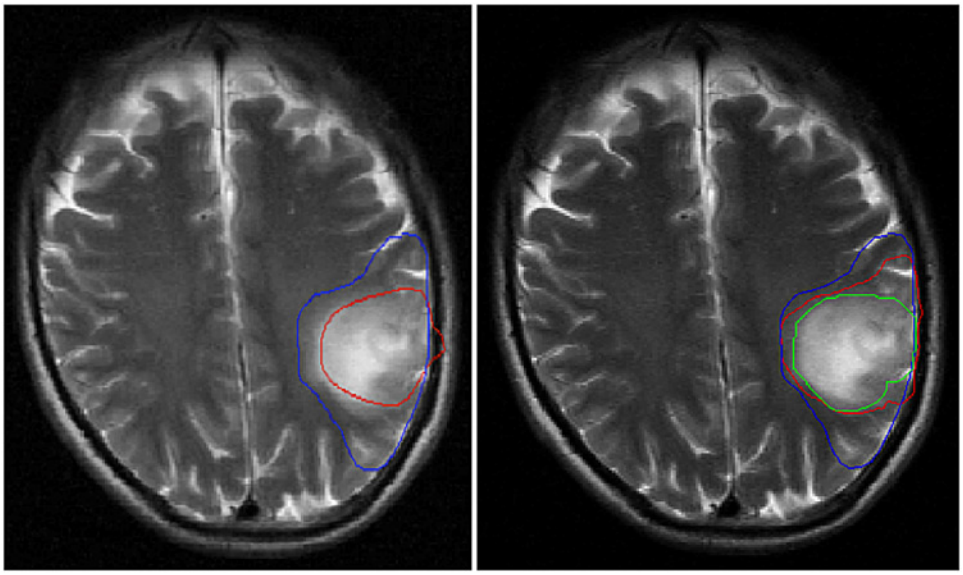

Fig. 2 *Left: Gaussian filtered MR image in which there is significant leakage of the level set contour (red line) at the meninges. Right: coherence enhanced diffusion filtered image and the resulting level set generated contour (red line) described in Section 2.4. The green contour was used as the initial front for level set evolution and in both images the blue contour is the GTV defined by an oncologist*

doi: 10.1049/htl.2015.0014

Table 1 Clinical characteristics of the patient cohort and the properties of the MR and CT data available for each patient

Case	Age/sex	Grade	Dose (Gy)/fractions	MR		CT	
				Series	Date	Slices	Date
1	46/M	II	60/30	T2 tse axial	17/07/2007	65	06/08/2007
2	46/F	III	60/30	T2 tse axial	18/07/2007	59	20/08/2007
3	54/M	IV	60/30	T2 tse axial	20/07/2007	63	13/08/2007
4	43/M	IV	60/30	T2 tse axial	27/08/2007	66	27/08/2007
5	50/M	II	60/30	T2 tse axial	20/09/2007	66	11/01/2008

by a clinical scientist (physicist) and a clinical oncologist. Patients were treated on a Varian 21EX linear accelerator with a prescription of 60 Gy in 30 daily fractions [23]. Table 1 shows the key clinical parameters of the patients included in this study.

2.2. Radiotherapy contouring: Contouring of the GTV and organs at risk (OAR) was performed by an experienced radiation oncologist using the Varian Eclipse™ (v6.5) treatment planning system (Varian Medical Systems, Inc. Palo Alto, CA, USA). Fig. 1 shows MR and CT images of grades II, III and IV brain tumours in the cohort. The CT images, which lack contrast and are difficult to interpret around the site of the tumour, show the GTV contour (inner red contour) and the planning target volume (PTV) (outer red contour). The GTV, CTV and OARs were defined according to the European Organisation for Research and Treatment of Cancer (EORTC) guidelines used in EORTC-26052. In these, the GTV is the resection cavity plus any residual enhancing tumour as seen on the radiotherapy planning CT images, which provide electron density information necessary for dose calculation, and pre- and post-operative MR images [24]. Since the registered MR was reconstructed in the same resolution and geometry as the corresponding CT, the resulting MR volume had the same number of image slices as the CT volume. As a result, the CT and MR image sets were used interchangeably to define the GTV, CTV and OARs [9, 10].

2.3. Noise removal and image smoothing: The acquisition of high-quality MR image data is limited by patient comfort during scanning. This result in a trade-off between resolution and signal-to-noise ratio for image acquisition in a clinically acceptable time frame, however, the effect can be reduced by post-processing noise reduction techniques [25–27]. The level set approach used in this work required conspicuous edge information because it uses gradient flow to evolve the image contours [28]. To remove noise, smooth small gaps in lines and curves, and to prevent boundary leakage at points of weak gradient, a coherence enhanced diffusion filter with optimised rotation invariance was used [29]. The advantage of this approach over Gaussian smoothing is that edges are better preserved while smoothing is limited. The significance of this is presented in Fig. 2, which shows the difference between a Gaussian and coherence enhanced diffusion filtered image and the resulting leakage using the level set approach described in Section 2.4.

2.4. Gradient-based level set method: Segmentation methods based on active contours or deformable models have been widely used in medical image analysis [30, 31]. The active contour (also known as a snake) evolves the initial contour by balancing two energy forces, the internal energy to impose a smoothness constraint and the external energy to push the contour towards desired features [30]. However, this formulation has difficulty in progressing into concave regions and unable to solve topological changes. Models of active contours within the framework of level sets have been developed to overcome these difficulties. Two such models, the Chan Vese (CV) [32] region-based model and the Chunming Li (CL) [28] model have obtained promising results in the segmentation of multi-modality medical image data [33–36]. Level set methods, which were first introduced by Osher and Sethian for capturing moving fronts, implicitly represent contours C_0 as the zero level set of an Lipschitz function ϕ defined in a higher dimension, usually referred as the level set function [37]. This is normally initialised as a signed distance function

$$u(x) = \begin{cases} \phi > 0 & \text{inside } C_0 \\ \phi < 0 & \text{outside } C_0 \\ \phi = 0 & \text{on } C_0 \end{cases} \quad (1)$$

From this, the level set function can be represented by

$$z = \phi(x, y, t = 0), \quad (2)$$

Differentiating with respect to time it follows that the implicit function that defines the motion of the curve is

$$\frac{\partial \phi}{\partial t} + u \cdot \nabla \phi = 0, \quad (3)$$

where u is the speed function defined in the normal outward direction. There are certain forms of speed function for different target segmentation tasks. As an alternative, the evolution partial differential equation of the level set function can be directly derived from the active contour formulation by minimising the energy function. This type of active contour, known as variational level set methods, is more convenient for incorporating information from edges or contours. The CV model is a typical region-based level set method, which handles local statistics and is therefore well suited for discontinuous contour segmentation. However, its performance in handling complete brain images has been unconvincing [34, 36]. The CL model is a gradient-based level set method, which finds edges evolving from the initial contour. It has inherent advantages when dealing with aggressive gliomas. Additionally, in traditional level set methods, a periodic reinitialisation of the level set function to a signed distance function must be done during evolution by solving the following reinitialisation equation [38, 39]

$$\frac{\partial \phi}{\partial t} = \text{sgn}(\phi_0)(1 - |\nabla \phi|). \quad (4)$$

However, this process can be eliminated by incorporating a third energy term that penalises the difference between the level set function and the signed distance function. This was defined by Li *et al.* [28] as

$$P(\phi) = \int_\Omega \frac{1}{2}(|\nabla \phi| - 1)^2 \, \mathrm{d}x \, \mathrm{d}y. \quad (5)$$

Since a signed distance function must satisfy the property of $|\nabla \phi| = 1$, by minimising the energy function in 5 it is

Table 2 Comparison of the clinical volumes defined by a radiation oncologist and the automatic volumes generated by the level set algorithm

	Case 1	Case 2	Case 3	Case 4	Case 5
clinical volume, cm^3	80.84	302.42	157.49	143.25	286.13
automatic volume, cm^3	72.69	265.93	157.38	114.38	213.65
volume difference, cm^3	8.15	36.49	0.11	28.87	72.66
difference, %	10.08	12.07	0.07	20.15	25.38
Dice coefficient ($\mu \pm \sigma$)	0.83 ± 0.07	0.74 ± 0.07	0.66 ± 0.1	0.74 ± 0.12	0.75 ± 0.07
Dice coefficient range (min, max)	0.71, 0.92	0.58, 0.82	0.51, 0.86	0.56, 0.94	0.71, 0.92
Hausdorff distance ($\mu \pm \sigma$), cm	0.95 ± 0.29	1.15 ± 0.47	1.39 ± 0.44	1.37 ± 0.63	1.86 ± 0.71
computation time, s	552	964	1301	907	913

straightforward to maintain this condition. In addition, an energy function may contain other terms that attract the contour such as a region-based [32] or shape-based prior [40]. In the CL model, a gradient is used to indicate edges by

$$g = \frac{1}{1 + |\nabla G_\sigma * I|^2}, \tag{6}$$

where I is the image grey level, and G_σ is the Gaussian kernel with standard deviation σ. The external energy that drives the zero level set to a target contour for a function $\phi(x, y)$ is $\varepsilon_{\text{external}}(\phi) = \lambda L_g(\phi) + \nu A_g(\phi)$, where $L_g(\phi)$ keeps the contour tight and $A_g(\phi)$ expands or shrinks the contour depending on the sign of this term. These are given by

$$L_g(\phi) = \int_\Omega g\delta(\phi)|\nabla\phi|\,\mathrm{d}x\,\mathrm{d}y, \tag{7}$$

$$A_g(\phi) = \int_\Omega gH(-\phi)|\nabla\phi|\,\mathrm{d}x\,\mathrm{d}y. \tag{8}$$

From (5) (7) and (8) the total energy function for the level set evolution is $(\partial\phi/\partial t) = -(\partial\varepsilon/\partial\phi)$, which more formally may be written as

$$\frac{\partial\phi}{\partial t} = \mu\left[\Delta\phi - \mathrm{div}\left(\frac{\nabla\phi}{|\nabla\phi|}\right)\right] + \lambda\delta(\phi)\mathrm{div}\left(g\frac{\nabla\phi}{|\nabla\phi|}\right) + \nu g\delta(\phi). \tag{9}$$

This gradient flow is the evolution equation of the level set function in the proposed method [28].

3. Experimental results: The methodology detailed in Section 2 was applied to the MR images of each patient to automatically determine the extent of the tumour. On each slice, the Dice coefficient and Hausdorff distance were calculated between the automatic and clinical contours used for treatment, the results of which are presented in Table 2. The mean Dice coefficient was found to be between 0.66 and 0.83, which indicates the range of geometric agreement between the clinical and automatically generated contours (Dice = 0 represents no agreement, 1 represents complete agreement). The mean Hausdorff distance was found to be between 0.95 and 1.86 also indicating good overall agreement between the clinical and automatically generated contours. Fig. 3 shows examples of typical contours produced by the algorithm (red line) and the corresponding contours produced by the clinical oncologist (blue line). Table 2 presents a comparison of the clinical volume and the volume produced by the algorithm. The clinical acceptability of the contours was also assessed with 7% graded as excellent, 60% as good and 33% as acceptable. None of the contours produced by the algorithm were found to be unacceptable.

4. Discussion: Accurately targeting radiotherapy to encompass infiltrated brain and at the same time limiting damage to important functional areas (e.g. hippocampus) is essential to reduce the risk of neurological deficit in glioma patients. However, accurately identifying the true extent of the tumour and important functional areas is extremely difficult. This is hampered by the fact that the GTV may appear different depending on the

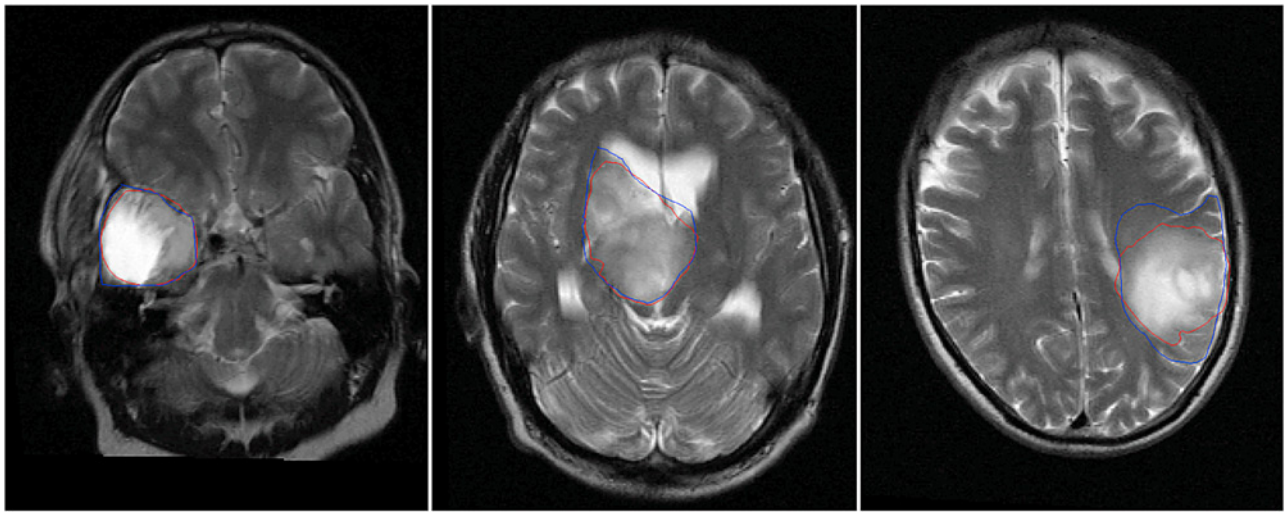

Fig. 3 *Comparison of clinical contours (blue) with typical contours produced by the algorithm (red), which were graded by an experienced clinician as excellent (left), good (middle) and acceptable (right)*

doi: 10.1049/htl.2015.0014

imaging sequences used [9, 10] and that in up to 50% of patients the tumour can grow during the interval between MR image acquisition and the start of radiotherapy [41]. In practical radiotherapy planning a margin of 2.5 cm is included around the tumour, however, with appropriately timed imaging and the availability of proven image analysis techniques for estimating the tumour volume this margin could potentially be reduced. It must also be borne in mind that significant clinical experience and judgement is required to determine the location of the GTV from the available MR and radiotherapy planning CT image data, which has limited soft tissue contrast. Furthermore, the addition of MR images to CT-based delineation may not reduce inter-observer variability. It is therefore important to use a combination of both when outlining brain tumours [42].

The difference between the automatic and clinical tumour volume was most significant in case 4, where a 20.15% difference corresponding to 28.87 cm^3 was recorded, and in case 5, where a 25.38% difference corresponding to 72.66 cm^3 was recorded. In both cases, the automatic volume was smaller than the clinical volume, a characteristic noted in all cases investigated. For case 5, the volume difference can be explained by the exceptionally long period of time, 114 days, between the MR and CT data acquisition. During this time, there was a significant change in the tumour burden of the patient, which although highlighted by the radiation oncologist on CT, was clearly not present at the time of MR acquisition. As a result, the level set approach was unable to evolve using tumour-specific grey-level information. Furthermore, unlike cases 1–4 in which a GTV was defined, a CTV was defined for this patient. The definition of a CTV on an image is a medical decision that is based on clinical judgement and experience and not simply on image information from different modalities, which is the approach used primarily to establish the GTV [9, 10]. As a result, the CTV contains the GTV and takes into account subclinical malignant disease relevant to the tumour site and treatment regime. The choice of microscopic infiltration outside of the GTV relies on integrating the biological and clinical behaviour of the region combined with knowledge of the surrounding anatomy. These characteristics, which are not taken into account in the method presented here, could be incorporated into future versions of the algorithm as an evolutionary constraint on the level set function.

One of the major advantages of this approach is that it is computationally efficient because the level set does not require reinitialisation during detection of the tumour boundary; a step that is often associated with slow convergence. The method relied on calculation of the gradient flow during evolution towards the tumour boundary. With the widespread variation in tumour intensity with glioma grade, and the difficulty in establishing gradients at the interface between tumour and normal tissue, there is a need to investigate level set evolution using the statistics of the region such as in the CV approach [32]. Furthermore, the performance of the approach could be improved by modelling the MR intensity variations using non-Gaussian statistical methods, particularly Rician methods, which have been widely used in MR analysis [25]. The approach presented used a posteriori information on tumour and organ at risk intensity to establish an adaptive active thresholding basis for level set evolution. Estimating the intensity range of a tumour and fitting to a model is difficult because tumour intensities may vary with tumour grade. Hence, more data is required to improve the efficacy of the approach in this area.

The importance of reducing PTV margins in glioblastoma multiforme (GBM) and the use of a more pragmatic definition of tumour volume that includes the imageable volume plus postoperative cavity was highlighted recently in a special issue of Clinical Oncology devoted to significant developments in neuro-oncology [8, 43, 44]. However, this depends on the ability to visualise the tumour, interpret radiological anatomy and recognise areas of tumour involvement. From the preliminary results presented, this image analysis approach, with further development, has the potential to assist clinicians with this task. However, more comprehensive analysis involving a much larger dataset is required. This will also help to address important issues surrounding the inclusion of MR data in the radiotherapy planning process, which does not necessarily reduce inter-observer variability and has been shown to result in larger tumour volumes than those produced using CT alone [42].

5. Conclusions: The proposed algorithm allows the tumour volume for radiotherapy to be estimated automatically and has the potential to be used by clinicians as an aid in outlining. The pilot results presented on five patients demonstrate the efficacy of the approach, however, full validation is required on a much larger dataset and using multiple observers to assess the automatically generated contours. The ultimate aim of this work is to develop an approach to assist clinicians define tumour volumes in a reliable and repeatable manner. This will not only save time but may reduce the radiotherapy fields used to treat brain cancer patients, which may be larger than necessary because of poor image information at the time of radiotherapy planning. This Letter reports our progress towards this aim and our ongoing work in this area.

6. Acknowledgments: The authors gratefully acknowledge the support of the staff in the Department of Oncology Physics for their help in preparation of the data used in this study and Dr Robin Grant, Consultant Neurologist, for helpful discussion about this work. The authors are also grateful to staff in the Institute for Digital Communications, College of Science and Engineering at the University of Edinburgh for their continuing support.

7. Funding and delaration of interest: The work was generously supported by NHS Lothian, Edinburgh and Lothians Health Foundation (charity number SC007342), the James Clerk Maxwell Foundation, the Jamie King Uro-Oncology Endowment Fund and a University of Edinburgh Darwin Award. Conflict of interest: none declared.

8 References

[1] DeAngelis L.M.: 'Brain tumours', *N. Engl. J. Med.*, 2001, **344**, pp. 114–123
[2] Deimling M. (Ed.): 'Gliomas recent results in cancer research' (Springer, 2009)
[3] Cancer Research UK: 'Cancer stats report – brain, other CNS and intracranial tumours key facts', January 2014
[4] Kleihues P., Burger P.C., Scheithauer B.W.: 'The new WHO classification of brain tumours', *Brain Pathol.*, 1993, **3**, pp. 255–268
[5] Krex D., Klink B., Hartmann C.: 'Long-term survival with glioblastoma multiforme', *Brain*, 2007, **130**, pp. 2596–2606
[6] Creak A.L., Tree A., Saran F.: 'Radiotherapy planning in high-grade gliomas: a survey of current UK practice', *Clin. Oncol. (R. Coll. Radiol.)*, 2011, **23**, pp. 189–198
[7] Ghose A., Lim G., Husain S.: 'Treatment for glioblastoma multiforme: current guidelines and Canadian practice', *Curr. Oncol.*, 2010, **17**, pp. 52–58
[8] Whitfield G.A., Kennedy S.R., Djoukhadar I.K., *ET AL.*: 'Imaging and target volume delineation in glioma', *Clin. Oncol.*, 2014, **26**, pp. 364–376
[9] ICRU 50: Prescribing, recording and reporting photon beam therapy, International Commission on Radiation Units and Measurements, Bethesda, MD, USA, 1993
[10] ICRU 62: Supplement to ICRU Report 50 'Prescribing, recording and reporting photon beam therapy', International Commission on Radiation Units and Measurements, Bethesda, MD, USA, 1999
[11] Mazzara G.P., Velthuizen R.P., Pearlman J.L., *ET AL.*: 'Brain tumor target volume determination for radiation treatment planning through automated MRI segmentation', *Int. J. Radiat. Oncol.*, 2004, **59**, pp. 300–312
[12] Angelini E.D., Clatz O., Mandonnet E., *ET AL.*: 'Glioma dynamics and computational models: a review of segmentation, registration, and in silico growth algorithms and their clinical applications', *Curr. Med. Imaging Rev.*, 2007, **3**, pp. 262–276

[13] Bauer S., Wiest R., Nolte L.P., *ET AL.*: 'A survey of MRI-based medical image analysis for brain tumor studies', *Phys. Med. Biol.*, 2013, **58**, pp. R97–129
[14] Zhou J., Rajapakse J.C.: 'Segmentation of subcortical brain structures using fuzzy templates', *Neuroimage*, 2005, **28**, pp. 915–924
[15] Dawant B.M., Hartmann S.L., Thirion J.P., *ET AL.*: 'Automatic 3D segmentation of internal structures of the head in MR images using a combination of similarity and free-form transformations. I. Methodology and validation on normal subjects', *IEEE Trans. Med. Imaging*, 1999, **18**, pp. 909–916
[16] Prastawa M., Bullitt E., Ho S., *ET AL.*: 'A brain tumour segmentation framework based on outlier detection', *Med. Image Anal.*, 2004, **3**, pp. 275–283
[17] Cuadra M.B., Pollo C., Bardera A., *ET AL.*: 'Atlas-based segmentation of pathological MR brain images using a model of lesion growth', *IEEE Trans. Med. Imaging*, 2004, **23**, pp. 1301–1314
[18] Wang T., Cheng I., Basu A.: 'Fully automatic brain tumour segmentation using a normalized Guassian Bayesian classifier and 3D fluid vector flow'. Proc. 17th Int. Conf. on Image Processing (ICIP), Hong Kong, China, 26–29 September 2010, pp. 2553–2556
[19] Corso J.J., Sharon E., Dube S.: 'Efficient multilevel brain tumor segmentation with integrated Bayesian model classification', *IEEE Trans. Med. Imaging*, 2008, **27**, pp. 629–640
[20] Ho S., Bullitt E., Gerig G.: 'Level-set evolution with region competition: automatic 3D segmentation of brain tumours'. Proc. of Int. Conf. on Pattern Recognition (ICPR), Quebec, Canada, 11–15 August 2002, pp. 532–535
[21] Zhu Y., Yan H.: 'Computerized tumor boundary detection using a Hopfield neural network', *IEEE Trans. Med. Imaging*, 1997, **16**, pp. 55–67
[22] Schmidt M., Levner I., Greiner R., *ET AL.*: 'Segmenting brain tumors using alignment-based features'. Proc. 4th Int. Conf. on Machine Learning and Applications (ICMLA), Los Angeles, CA, USA, 15–17 December 2005, pp. 215–220
[23] Bomford C.K., Kunkler I.H.: 'Walter and Miller's textbook of radiotherapy: radiation physics, therapy and oncology' (Churchill Livingston, 2003)
[24] EORTC-26052: 'Phase III trial comparing conventional adjuvant temozolomide with dose-intensive temozolomide in patients with newly diagnosed glioblastoma'. Radiation Therapy Oncology Group (RTOG). Available at https://www.clinicaltrials.gov/ct/show/NCT00304031
[25] Nowak R.D.: 'Wavelet-based Rician noise removal for magnetic resonance imaging', *IEEE Trans. Image Process.*, 1999, **8**, pp. 1408–1419
[26] Macovski A.: 'Noise in MRI', *Magn. Reson. Med.*, 1996, **36**, (3), pp. 494–497
[27] Nobi M.N., Yousuf M.A.: 'A new method to remove noise in magnetic resonance and ultrasound images', *J. Sci. Res.*, 2001, **3**, (1), pp. 81–89
[28] Li C., Xu C., Gui C., *ET AL.*: 'Level set evolution without re-initialization: a new variational formulation'. Proc. of IEEE Conf. on Computer Vision and Pattern Recognition (CVPR), San Diego, CA, USA, 20–26 June 2005, pp. 3243–3254
[29] Weickert J., Scharr H.: 'A scheme for coherence-enhancing diffusion filtering with optimized rotation invariance', *J. Vis. Commun. Image Represent.*, 2002, **13**, pp. 103–118
[30] Kass M., Witkin A., Terzopoulos D.: 'Snakes: active contour models', *Int. J. Comput. Vis.*, 1997, **1**, pp. 321–331
[31] Cootes T.F., Taylor C.J., Cooper D.H.: 'Active shape models their training and application', *Comput. Vis. Image Und.*, 1995, **61**, pp. 38–59
[32] Chan T.F., Vese L.A.: 'Active contours without edges', *IEEE Trans. Image Process.*, 2001, **10**, pp. 266–277
[33] Kozic N., Weber S., Buchler P., *ET AL.*: 'Optimisation of orthopaedic implant design using statistical shape space analysis based on level sets', *Med. Image Anal.*, 2010, **14**, pp. 265–275
[34] Dietenbeck T., Alessandrini M., Barbosa D.: 'Detection of the whole myocardium in 2D-echocardiography for multiple orientation using a geometrically constrained level-set', *Med. Image Anal.*, 2012, **16**, pp. 386–401
[35] Baillard C., Hellier P., Barillot C.: 'Segmentation of brain 3D MR images using level sets and dense registration', *Med. Image Anal.*, 2001, **5**, pp. 185–194
[36] Scherl H., Hornegger J., Prummer M., *ET AL.*: 'Semi-automatic level-set based segmentation and stenosis quantification of the internal carotid artery in 3D CTA data sets', *Med. Image Anal.*, 2007, **11**, pp. 21–34
[37] Sethian J.A.: 'Level set methods and fast marching methods: evolving interfaces in computational geometry, fluid mechanics, computer vision, and materials science' (Cambridge University Press, 1999, 1st edn.)
[38] Caselles V., Catte F., Coll T., *ET AL.*: 'A geometric model for active contours in image processing', *Num. Math.*, 1993, **66**, pp. 1–31
[39] Caselles V., Kimmel R., Sapiro G.: 'Geodesic active contours', *Int. J. Comput. Vis.*, 1997, **22**, pp. 61–79
[40] Vemuri B.C., Ye J., Chen Y., Leonard C.M.: 'Image registration via level-set motion: applications to atlas-based segmentation', *Med. Image Anal.*, 2003, **7**, pp. 1–20
[41] Pennington C., Kilbride L., Grant R., *ET AL.*: 'A pilot study of brain tumour growth between radiotherapy planning and delivery', *Clin. Oncol.*, 2006, **18**, pp. 104–108
[42] Weltens C., Menten J., Feron M., *ET AL.*: 'Interobserver variations in gross tumor volume delineation of brain tumors on computed tomography and impact of magnetic resonance imaging', *Radiother. Oncol.*, 2001, **1**, pp. 49–59
[43] Burnet N.G., Jena R., Burton K.E., *ET AL.*: 'Clinical and practical considerations for the use of intensity-modulated radiotherapy and image guidance in neuro-oncology', *Clin. Oncol.*, 2014, **26**, pp. 395–406
[44] Rampling R., Erridge S.: 'Management of central nervous system tumours in the elderly', *Clin. Oncol.*, 2014, **26**, pp. 431–437

doi: 10.1049/htl.2015.0014